A 3D Visualization and Guidance System for HandHeld Optical Imaging Devices

Fred S. Azar[1], Benoit de Roquemaurel[1],
Albert Cerussi[2], Nassim Hajjioui[1], Ang Li[2], Bruce J Tromberg[2], Frank Sauer[1]

[1]Siemens Corporate Research, 755 College Road East, Princeton, NJ 08540
[2]University of California, Irvine, CA 92697

ABSTRACT

We have developed a novel 3D visualization and guidance system for handheld optical imaging devices. In this paper, the system is applied to measurements of breast/cancerous tissue optical properties using a handheld diffuse optical spectroscopy (DOS) instrument. The combined guidance system/DOS instrument becomes particularly useful for monitoring neoadjuvant chemotherapy in breast cancer patients and for longitudinal studies where measurement reproducibility is critical. The system uses relatively inexpensive hardware components and comprises a 6 degrees-of-freedom (DOF) magnetic tracking device including a DC field generator, three sensors, and a PCI card running on a PC workstation. A custom-built virtual environment combined with a well-defined workflow provide the means for image-guided measurements, improved longitudinal studies of breast optical properties, 3D reconstruction of optical properties within the anatomical map, and serial data registration. The DOS instrument characterizes tissue function such as water, lipid and total hemoglobin concentration. The patient lies on her back at a 45-degrees angle. Each spectral measurement requires consistent contact with the skin, and lasts about 5-10 seconds. Therefore a limited number of positions may be studied. In a reference measurement session, the physician acquires surface points on the breast. A Delaunay-based triangulation algorithm is used to build the virtual breast surface from the acquired points. 3D locations of all DOS measurements are recorded. All subsequently acquired surfaces are automatically registered to the reference surface, thus allowing measurement reproducibility through image guidance using the reference measurements.

Keywords: Image-guided procedures, clinical applications, longitudinal studies, breast imaging, chemotherapy monitoring, image registration, handheld imaging devices, optical imaging.

1. INTRODUCTION

Recent work at the Beckman Laser Institute has reported the first use of DOS to track tumor response to neoadjuvant chemotherapy in a human subject [11]. Significant reductions in total tumor hemoglobin (ctTHb) and water content of 56% and 67%, respectively were observed by the end of the treatment. In addition, lipid content increased by nearly 28%. Recent DOI studies have supported these findings by comparing optical imaging with MRI [17,18] and ultrasound [19] after long-term treatment. A recent study has also demonstrated that changes in DOS-measured hemoglobin and water may predict which tumors may demonstrate pathological response only one week after the start of therapy [16]. We believe that DOS may report upon on endogenous *in vivo* "biomarkers" that report on tissue biochemical status that may predict the degree of pathological response in treated tumors. Although DOS-measured parameters such as deoxy-hemoglobin and water lack the specificity of genetic biomarkers, DOS-measured parameters nevertheless report on tissue vascular status, which is an important aspect of anti-cancer therapies (i.e., angiogenesis). Measuring tumor hemoglobin concentrations,

Medical Imaging 2007: Visualization and Image-Guided Procedures, edited by Kevin R. Cleary, Michael I. Miga,
Proc. of SPIE Vol. 6509, 650909, (2007) · 1605-7422/07/$18 · doi: 10.1117/12.710506

oxygenation, and water content *in vivo* could facilitate clinical trials in pre-clinical animal models (i.e., drug discovery), or by providing optimized individual response assessment in humans.

The DOS measurements described below use a simple handpiece reflectance geometry, similar to an ultrasound. Although a handheld probe affords several advantages over fixed imaging geometries, some key problems exist. Many of these limitations have been addressed in the ultrasound literature. For example, there is concern of operator-dependent measurements. The tissue/probe coupling is also a concern and artifacts manifest due to improper probe handling. Sampled volume differences between scans and operators offer another challenge. In addition, co-registration between imaging modalities (i.e., optics and MRI) can be problematic because of differing tissue-sampled volumes and varying patient positions. Note that these problems are *amplified in longitudinal measurements*, *since significant day-to-day coupling variations produce artifacts*. It is critical to ensure that the ROI's and probe-tissue-orientation are consistent for longitudinal measurements, especially as the strength of the optical signals decrease. Consistent longitudinal measurements have been performed with our instrumentation, but great care was taken to ensure that the same operator performed each measurement.

Our answer to these challenges was to construct a 3D visualization and guidance system for handheld optical imaging devices. This prototype has been have applied to the DOS system developed by Professor Bruce Tromberg's team at the Beckman Laser Institute, U. of California, Irvine. The tracking system offers the consistency required for a clinical standard and by removing any operator-dependent tendencies permits DOS instrument testing in multi-center clinical trials. The tracking system will improve the sensitivity of the method to smaller and more obscure physiological signals. In addition, the tracking system will dramatically improve efforts for co-registration to help validate optical methods, cross validate optical imaging techniques with each other, and facilitate multi-modality imaging in general. The benefits of the tracking system will improve the reliability of <u>any</u> handheld optical probe, such as those engineered for flow, or optical probes combined with ultrasound.

In the present study, we provide a quick overview of DOS technology in section 2. The workflow and the architecture of the guidance system software are described in section 3. Depending on whether a reference surface and measurements have been already completed, or whether the magnetic tracker is operational, three specific workflows are defined, and follow different steps: sensor calibration, building local system of coordinates, scanning surface, measurements and alignment. These modules are developed in section 4.

2. DOS TECHNOLOGY

2.1. What is Diffuse Optical Spectroscopy?

Diffuse optical spectroscopy (DOS) is a non-invasive, bedside technique that quantitatively measures near-infrared (NIR) (650 to 1000 nm) absorption and reduced scattering spectra [1]. Absorption spectra are used to calculate the tissue concentrations of oxygenated (ctO2Hb) and reduced hemoglobin (ctHHb), water (ctH2O), and lipid, which are the dominant near-infrared (NIR) molecular absorbers in breast. Recent evidence has uncovered additional biochemical shifts in NIR absorption spectra due to water, lipids, and hemoglobin breakdown products, which may provide specific quantitative information about tumor biochemistry [2-4]. DOS does not require exogenous contrast, although exogenous agents can and have been developed. DOS rapidly (e.g. few seconds) provides quantitative, functional information about tumor biochemical composition with a handheld probe, making it potentially desirable from a patient perspective. Typically, DOS samples a low number of spatial locations with a large spectral bandwidth. In contrast, Diffuse Optical Imaging (DOI) typically samples a large number of spatial locations but with low spectral bandwidth. The relationship between DOS and diffuse optical imaging (DOI) is comparable to that of magnetic resonance spectroscopy (MRS) and magnetic resonance imaging (MRI).

2.2. The Uses of Broadband Spectroscopy

Within the NIR spectral region hemoglobin is a well-known molecular absorber, and a frequent target of optical spectroscopy. However, there are many other potentially important endogenous molecular targets available

through NIR tissue spectroscopy. Water (ctH2O), and lipids are abundant in breast tissues [7,8]. Ignoring water concentrations in tissues can lead to oximetry errors, especially for instruments with a low number of wavelengths [9]. Alterations in lipid and water biochemistry also require broadband information content [2,4]. Broadband spectral characterization is necessary in order to extract the maximum number and type of quantitative optical biomarkers from the tissue.

2.3. Handheld Instrument Design

Research at the Laser Microbeam and Medical Program (LAMMP, an NIH Technology Resource Center) has produced the Laser Breast Scanner (LBS), a bedside translational research device that is currently active in clinical applications. Figure 1 presents a schematic of the clinical LBS instrument, which has been described at length in the literature.[5,10]. The LBS employs multiple laser diodes that provide visible/NIR light at discrete wavelengths (660, 680, 780, 808, 830, and 850 nm) for the frequency-domain measurement of tissue absorption and scattering. An integrated steady-state spectrometer system allows us to expand the measurement quantitatively from 600 to 1000 nm. Proper modeling of both frequency-domain and steady-state systems yields an absolute broadband tissue absorption spectrum which is de-convolved from tissue scattering.

Only a handheld probe is in contact with the patient (Figure 2). This probe has been designed to house an avalanche photodiode (APD) that records frequency-domain optical signals after tissue interrogation. An optical fiber (labeled "SSFDPM" in Figure 2) delivers detected spectra to the spectrometer. The total measurement time is 5-10 seconds/location. The entire system is cart-based. The source-detector separation, and hence the probing depth, can be changed by sliding the source fibers along a grooved track. The reflection-style geometry is similar to an ultrasound probe.

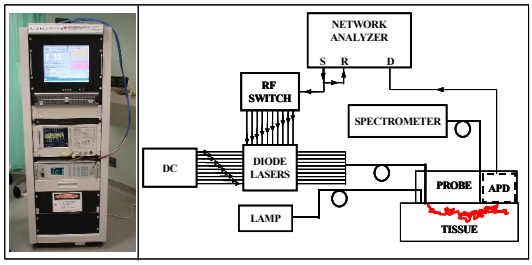

Figure 1 – Design of the current LBS instrument (DOS). The clinical system combines discrete-wavelength FDPM and broadband steady-state spectrometers.

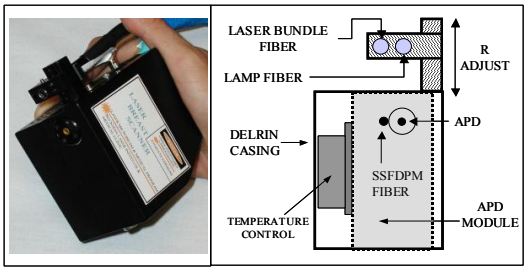

Figure 2 – Current LBS handpiece configuration. The right panel shows the two source fibers and the two detection optics (fiber and APD). Temperature control is a DC fan plus a temperature control element.

3. WORKFLOW & ARCHITECTURE

3.1. Example of DOS in monitoring breast cancer

This case study was the first documented use of DOS to track the progression of neoadjuvant chemotherapy in a human subject [11]. A 54 year old post-menopausal Caucasian female with a previous right mastectomy underwent neoadjuvant therapy for cancer of the left breast. The tumor was palpable in the lower inner quadrant and diagnosed as adenocarcinoma by fine needle aspiration. Two weeks before treatment, mammography revealed a 2.3 x 2.5 cm mass with microcalcifications. The patient began 3 cycles spaced 3 weeks apart of a doxorubicin/cyclophosphamide (A/C) drug combination. The tumor was judged nonpalpable at the conclusion of the 3 cycles. Surgical pathology revealed a stellate fibrotic lesion measuring 2.0 x 1.0 x 1.0 cm with a 5 mm residual tumor within the fibrosis.

A series of DOS linescans were performed spanning 68 days and 3 treatment cycles. In the 1st chemotherapy cycle, linescans were obtained immediately prior to chemotherapy treatment (day 0) and daily (days 3, 4, 5, 6, 7) thereafter. Additional linescans were measured on days 24 and 26 and 68 (i.e., 13 days prior to surgery). Temporal changes in tumor water are plotted in Figure 3a along with control measurements from the abdomen

and the left upper outer quadrant of the breast. Values over the tumor steadily decreased, and approached the control values. After 10 weeks, the maximum tumor water volume concentration dropped 67% from its original value (41 ± 9 % to 13.7 ± 0.7 %), whereas control measurements did not change significantly (5.9 ± 0.3 % to 5.8 ± 0.3 %). The greatest changes occurred within the first week (37% decreases).

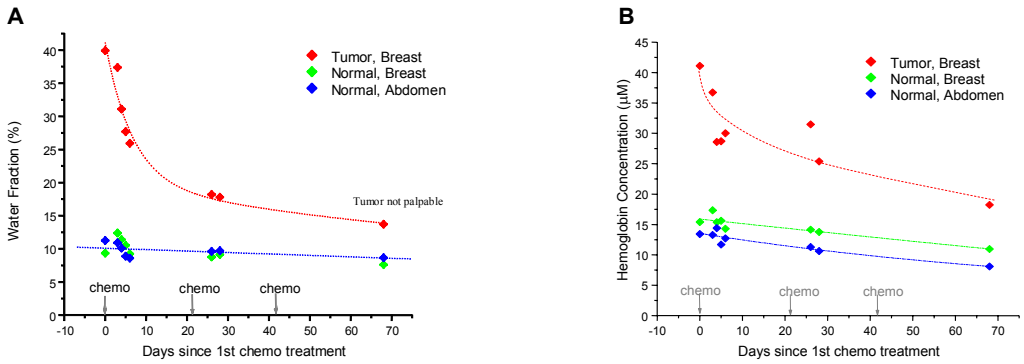

Figure 3 – Changes in tumor and normal tissues resulting from neoadjuvant chemotherapy. Large early changes are seen in both tissue water (A) and total hemoglobin concentration (B). Note that tumor approaches control as the therapy progresses. The slightly decreasing controls in (B) resulted from a systematic decrease in hematocrit.

Tumor total hemoglobin concentrations (ctTHb) also dropped substantially during therapy (Figure 3b). Over 10 weeks, ctTHb dropped from 41 ± 3 μM to 18.2±0.9 μM, a 56% decrease. Again, approximately half of the drop occurred within the first week (26%; to 30±2 μM). Normal breast dropped 32% (16±1 to 11±2 μM) and the abdomen dropped 40% (13.4±0.7 to 8.1±0.8 μM). These decreases in control tissues implied a systemic hemoglobin drop, which was verified by invasive blood sampling (36.7% to 30.7% in hematocrit). The decreasing trend in control hemoglobin was mainly due to ctO2Hb: control measurements of ctHHb varied minimally over the entire treatment course (5.1 ± 0.8 to 6.1 ± 0.3 μM) compared to the relatively large change in ctO2Hb (11 ± 1 to 5 ± 2 μM; 57% drop). The same trend is present in control abdominal measurements.

The water content measured over the tumor (ctH2O) increased, as expected, for a cellular mass located in a lipid-rich background. Our measured decrease in tumor hemoglobin is compatible with reductions observed in angiogenesis studies verified by pathology [12]. In addition, elevated water content of tumors is an indication of local edema and/or necrosis. The decrease in water concentration resulting from therapy may also be associated with cellular apoptosis induced via chemotherapy, as some MRI measurements have suggested [13]. Tumor control water/lipid ratios dropped 4.4-fold, which is in excellent agreement with previous findings from MRS which demonstrated a 4.3-fold decrease over the course of 3 chemotherapy cycles [14]. DOS and MRI retrieve highly correlated water and lipid concentrations from tissue-simulating phantoms [15].

3.2. Workflows

This experiment demonstrates two important facts: quantitative optical biomarkers (a) can track biochemical kinetics in tumors using a DOS handheld probe, and (b) significant biochemical changes occur in as little as a few days after the first course of treatment. In order to use this method in a clinical environment, one has to develop a guidance and visualization system to facilitate and certify the ease, repeatability and accuracy of such a technique.

We have defined three workflows corresponding to the different processes a patient can go through:

A. The first time a patient comes in, a first scan of the breast surface is completed (the *reference scan*) and measurements are done. The shape of the surface and the position of the measurements are stored following the steps:

1. Calibration of the sensors if necessary,
2. Scan the surface of the breast,
3. Acquire new measurements,
4. Store data.

B. The following handheld scans are based on the *reference* surface and measurements: a new surface (the *current scan*) is scanned. In order to compare the results on the *reference* and *current* surface, one performs the following steps:
   1. Calibrate sensors if necessary,
   2. Load *reference* surface and measurements,
   3. Scan the *current* surface,
   4. Align the *current* surface to the *reference* surface: the *reference* measurements are projected onto the *current* surface (virtual measurements),
   5. Acquire new measurements based on the location and orientation of the *current* measurements,
   6. Delete virtual measurements,
   7. Store data.

C. One can also compare the results of different examinations. This can be done with or without the magnetic tracker:
   1. Load *reference* surface and measurements,
   2. Load *current* surface and measurements,
   3. Align surfaces,
   4. Evaluate results.

These three simple workflows are a synthesis of the requirements of guidance system. Then, these characteristics present some challenging requirements. The system should meet the following criteria:
1. Simple usage in a clinical environment
2. Provide 6-axis tracking (three axes for position and three for orientation)
3. Real time feedback
4. 5mm maximum positional precision
5. Not interfere with the normal use of the optical probe
6. Economical
7. Easily integrated into existing optical handheld probe instruments

3.3. Architecture

To be able to build a software platform that can implement the three workflows presented in section 3.2, we must now describe the technical choices (tracking devices) and the architecture of HandHeld.

3.3.1. Tracking sensors

We use a magnetic tracking system from Ascension Technologies which is easy to integrate into our system and accurate enough even if as every magnetic tracking device, it is susceptible to distortion. The magnetic tracker system from Ascension Technologies is composed of a PCI card, a magnetic base and three sensors. Every sensor provides spatial measurements as 6 parameters corresponding to the location and direction of the sensor. Three sensors are used for the following purposes:
1. A first sensor is used with a thin pointing rod, rigidly attached to the sensor. This sensor is used to scan the surface of the breast.
2. The second sensor is rigidly attached to the DOS handheld instrument. This sensor is used to do locate the measurements on the breast.
3. The third sensor is appropriately taped to the patient a few inches above the xyphoid process in order to account for patient body movements (e.g. breathing) with respect to the transmitter position.

Sensors #1 and #2 must be calibrated: the position of the instrument extremity should be known in a system of coordinates linked to the sensors.

3.3.2. Structure of the guidance system

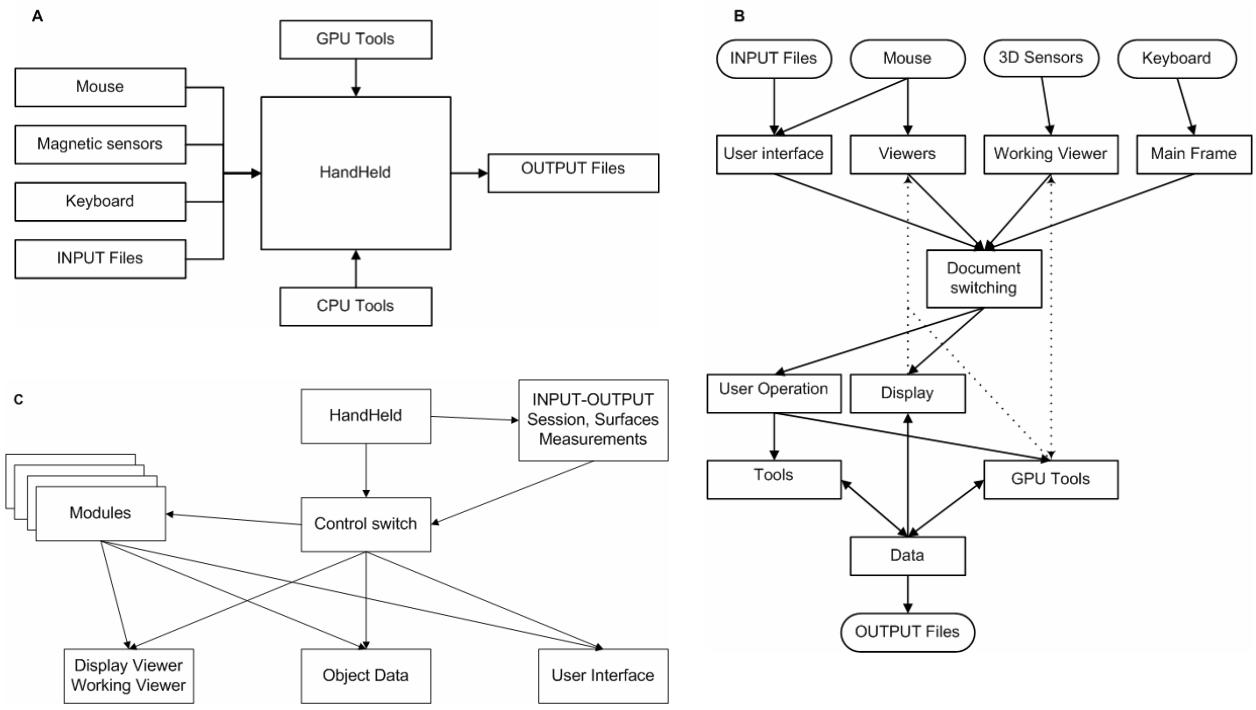

Figure 4 – A. Input and Output of the system. B. Main data and control streams. C. Static architecture of the system.

The software guidance and visualization system has to deal with numerous inputs as shown in Figure 4A. The events to deal with are the usual mouse and keyboard but also the magnetic sensors. Another challenge is also computation of large amounts of data (e.g. projection of sensor on surface in section 4.3). To be able to meet the live constraints and for a better display, we use the graphics processing unit (GPU) power. Then, the working viewer is added to the architecture. As a viewer, it can manage a stack of events from the 3D sensors and can have GPU buffers which are not displayed but are used for GPU tools. In order to use the magnetic sensors as 3D mice which interact with the working viewer, their behavior is implemented in a thread that sends messages to the working viewer. The static architecture of the system is represented in Figure 4C: the application is composed of a control switch, three main blocks: display viewer and working viewer, object data and user interface (buttons for users), some modules to make links between the three main blocks and an input-output block to load and store sessions, surfaces and measurements position.

Since the system is highly interactive, it is quite challenging to insure a stable software platform. As shown in Figure 5, we have defined states and transitions to fit the workflows defined in section 3.2. These states and transitions are taken into account in the document switching or control switch in Figure 4B and Figure 4C. The states with double line correspond to initial states; the states with thick line to final states.

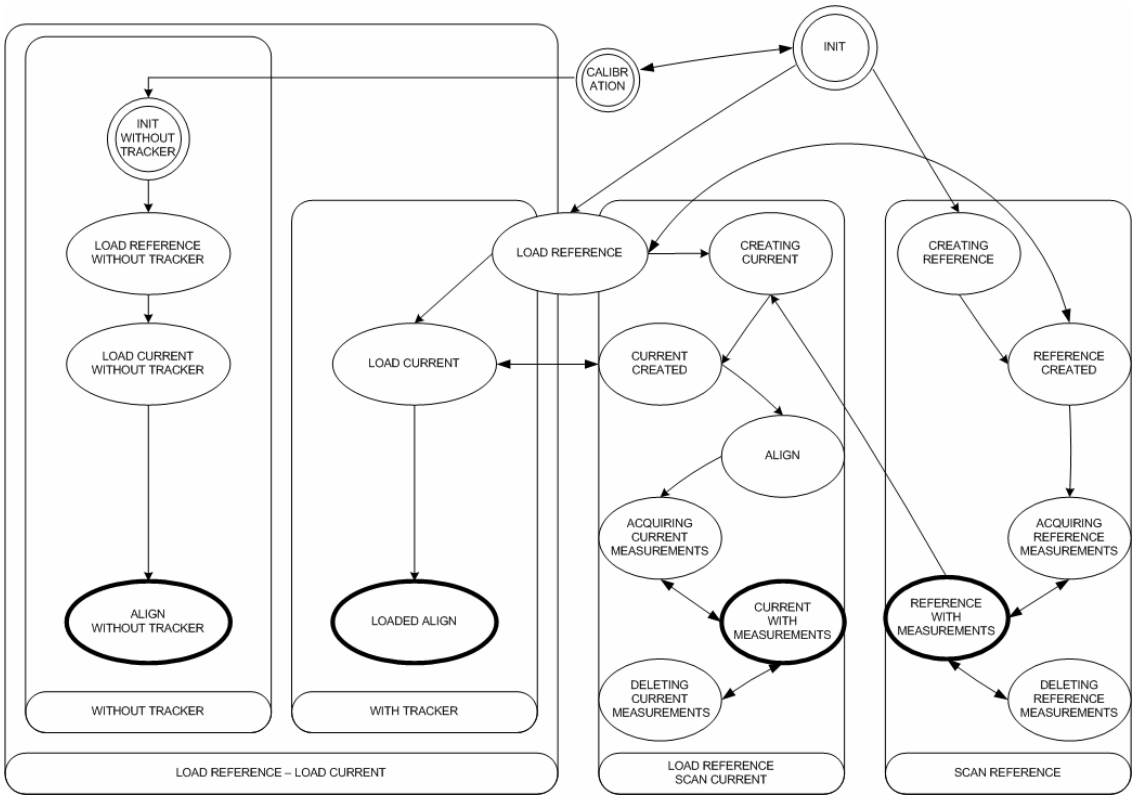

Figure 5 – States and main transitions of the system.

.

4. KEY MODULES

The workflows introduced in section 3.2 and explicit in Figure 5 involve several modules (introduced in Figure 4C). These modules offer ease to the operator and a high level of interactivity. These modules are the following.

4.1. Calibration of sensors

This module corresponds to a compulsory step before using the sensors (sensor #1 or #2 described in section 3.3.1). Each tracking device gives a set of 6 data corresponding to the position and direction of the magnetic sensor. Each sample of data $M = (R, T)$ is composed of T the position of the sensor in a system of coordinates linked to the magnetic base and R a rotation matrix which axis the main direction of the tracker. The calibration process consists into finding a vector C so that for each point M, the position P of the instrument tip is given by $P = RC + T$.

During the calibration process, the instrument tip should be fixed on a point and the device should be allowed to rotate around that point. Let's $(M_i = R_i, T_i)$ be the sample points. One can approximate the calibration vector C as a least-square minimization:

$$\sum_{i \neq j} \left\| R_i C + T_i - R_j C - T_j \right\|^2$$

The solution C can be written as:

$$C = \left(RR^T RR \right)^{-1} RR^T TT \text{ where } RR = \left[\ldots R_i - R_j \ldots \right] \text{and} \, TT = \left[\ldots T_i - T_j \ldots \right]$$

4.2. Scanning surfaces

When the sensors are calibrated, one can use the sensor #1 (thin pointing rod) to scan a surface. We divide the scan of surface into three main steps.

4.2.1. Building patient coordinate system

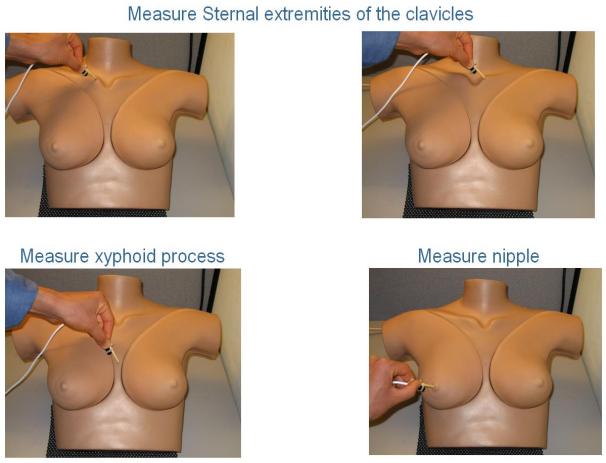

Figure 6 – Building the patient coordinate system: magnetic sensor records position of several anatomical landmarks

Since the patient will not lie in the same position on the chair were the measurements are taken, one must first build a patient coordinate system based on some well-know anatomical landmarks. 4 points are then scanned as shown in Figure 6:

- Sternal extremity of the left clavicle S_L
- Sternal extremity of the right clavicle S_R
- Xyphoid process P_X
- Nipple N

The first three points defined the orientation of the axis of the new coordinates system and nipple as the origin and the sense of the new coordinates $\left(N, \vec{i}, \vec{j}, \vec{k}\right)$:

$$\vec{k} = \pm \frac{\overrightarrow{S_L P_X} \otimes \overrightarrow{S_R P_X}}{\left\| \overrightarrow{S_L P_X} \otimes \overrightarrow{S_R P_X} \right\|} \text{ and } \vec{k}.\overrightarrow{P_X N} \geq 0$$

$$\vec{j} = \frac{\overrightarrow{P_X S_L} + \overrightarrow{P_X S_R}}{\left\| \overrightarrow{P_X S_L} + \overrightarrow{P_X S_R} \right\|} \text{ and } \vec{i} = \vec{j} \otimes \vec{k}$$

4.2.2. Scanning the breast

From now on, the sensor #3 will correct the position of others sensors to prevent patient movement from modifying results. As shown on Figure 7, one draws a number of curves centered around the nipple

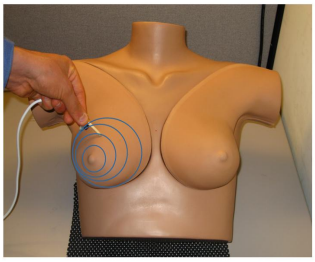

Figure 7 – Generating the surface mesh of the breast

4.2.3. Creating the mesh

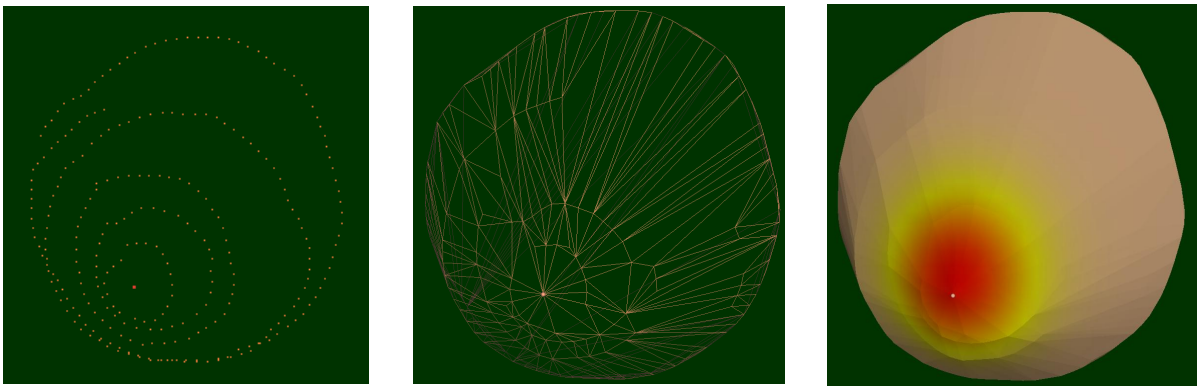

Figure 8 – Generated mesh: (*from left to right*): tracked points, the mesh and the surface with texture

As a first approximation, one uses the convex envelope of the points cloud obtained at section 4.2.2. To do this, one proceeds to the 3D Delaunay triangulation of the points cloud and selects the facets of tetrahedron of the Delaunay triangulation that belongs to only one tetrahedron. This method is not perfect since the breast surface may not be convex. Some more complex algorithms are on their way to be developed. The results can be seen in Figure 8. To have a better display and anticipating more complicated meshes of surfaces, one uses vertex buffer objects to limit the data stream between CPU and GPU memory. Surfaces are stored as sets of triangles.

4.3. Measurements

Figure 9 – Measurements

As shown in Figure 9, one uses the sensor #2 with the DOS instrument at its extremity. While doing measurements, the position of the active part of sensor #2 (corrected by sensor #3 which models the patient movement) is projected onto the surface. Then, measurements can be finalized or removed.

4.3.1. Projection of the sensor onto the surface

The projection onto the surface is done by an algorithm that projects the point onto each triangle (orthogonal projection inside the triangle or orthogonal projection on the edges or the closest vertices of the triangle).

One also computes the position of the instrument extremity relatively to the surface. Knowing the triangle ABC and its normal $\vec{N}$ exiting the volume, the extremity P of the instrument is outside the volume if $\overrightarrow{AP}.\vec{N} \geq 0$. If P is inside, it means that the operator put too mush pressure on the breast and deform it, what modifies measurements position. In the same way, the distance between the point P and its projection allows to have a better idea of how far the instrument is from the surface.

4.3.2. Adding measurements

When measurements are done, two situations occur:

- Measurements are done on the reference surface. Then, one must only focus on the location of the measurements which are done near the tumor.
- Measurements are done on the current surface. One has to redo measurements in the exact same location as done on the reference surface. As explained in section 3.2, the measurement positions are projected on the current surfaces and these virtual measurements guide the operator to do the measurements. Then, two parameters are essential in this situation: the distance to the surface but also the distance to the virtual corresponding measurement and its orientation. As could be seen in Figure 10, a tip is displayed on the screen to be sure that not only the position but also the direction corresponds.

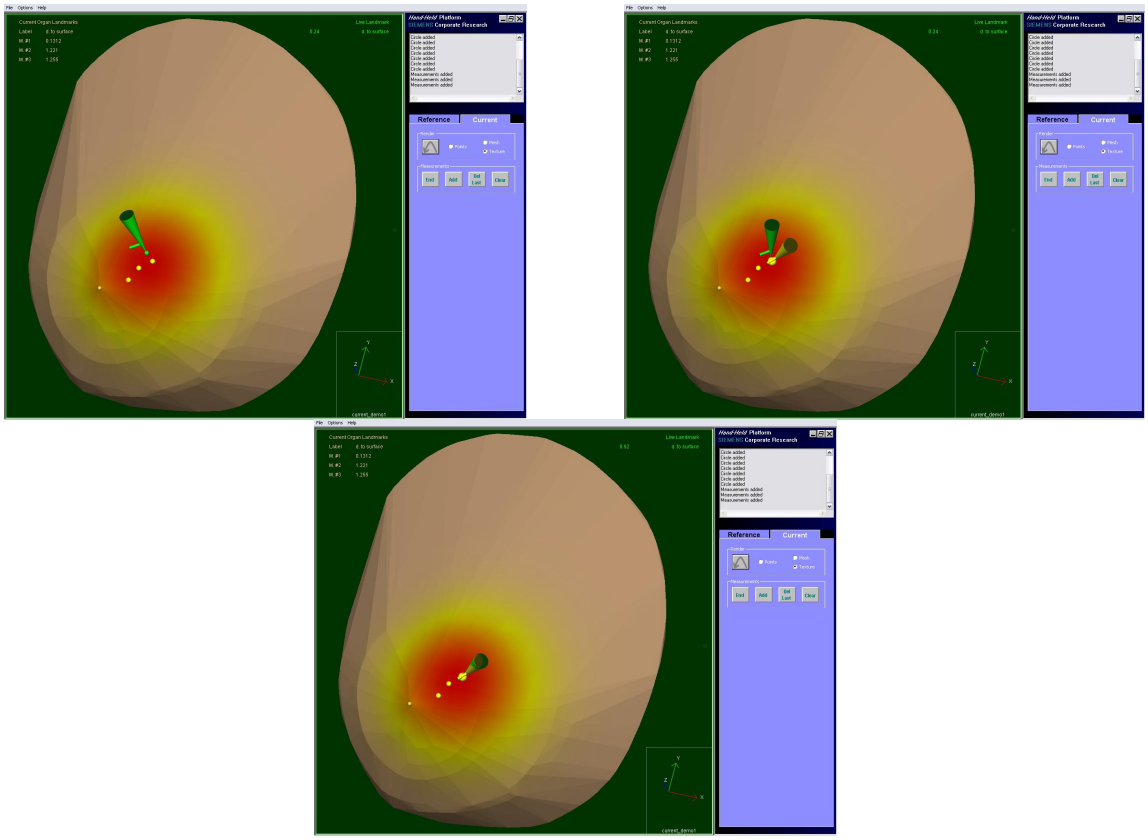

Figure 10 – Add measurements on the current surface: (*From left to right and top to bottom*) the projection is green on the surface, when getting closer to the virtual measurements, the direction yellow cone is displayed; the two cones match, one can add the two measurements.

4.3.3. Deleting measurements

There are two possibilities to delete measurements. In measurement mode, one can delete the last measurements. Or, if measurements are done, a picking algorithm has been implemented and can be used to delete one by one the location of the measurements on the screen.

4.4. Alignment

We have defined the patient coordinate system in section 4.2.1, two different patient coordinate systems exist when we compare reference and current surfaces. In order to take into account the difference of positions of the patient between the two sessions, we must align the coordinate systems to one another. Actually, in order to simplify the computation, the reference surface is aligned to the current.

4.4.1. Two types of alignment

We have implemented two types of rigid alignment (i.e. Rotation and translation to apply to the current surface):

- An alignment of 3 landmarks to 3 landmarks defined in section 4.2.1 since these three landmarks are well defined.
- An alignment of the point of the reference surface to the triangles of the current surfaces even if these methods seem to depend too much on the choice of tracked points.

When the rigid transformation is computed, all data of the reference surface is then expressed into the current coordinate surface.

4.4.2. Creation of virtual measurements

When the two surfaces are in the same coordinate system, it is then possible to projects the reference measurements location onto the current surface using the projection algorithm proposed in section 4.3.1. The results of these projections are virtual measurements used to guide the adding measurements in section 4.3.2.

5. CONCLUSION

The guidance and visualization system presents good initial results and seems to be quite stable. However, some work remains such as introducing the third sensor whose role is to correct the position of the other two sensors from patient movements and developing a better and more general algorithm to generate surface mesh. These improvements should be easy since the architecture has been designed for expansion. Finally, additional tests must be done on thesystem to check if its accuracy corresponds to the requirements.

REFERENCES

[1] Sevick, E. M., Change, B., Leigh, J., Nioka, S. and Maris, M., "Quantitation of time-resolved and frequency-resolved optical spectra for the determination of tissue oxygenation," Anal. Biochem., vol. 195, pp. 330-51, 1991.

[2] Kukreti, S., Cerussi, A., Tromberg, B. and Gratton, E., "Intrinsic markers revealed by a novel spectral analysis of near-ir spectra of breast tumors," presented at San Antonio Breast Cancer Research Symposium, San Antonio, TX, 2006.

[3] Kukreti, S., Cerussi, A., Tromberg, B. and Gratton, E., "Intrinsic near infrared spectroscopic markers of breast tumors," Disease Markers, vol. accepted for publication, pp., 2006.

[4] Merritt, S. I., Sakurai, R., Cerussi, A. E., Durkin, A. J. and Tromberg, B. J., "Monitoring deep tissue temperature with broadband diffuse optical spectroscopy," in BiOS 2005, San Jose, CA: International Society for Optical Engineering, 2005.

[5] Bevilacqua, F., Berger, A. J., Cerussi, A. E., Jakubowski, D. and Tromberg, B. J., "Broadband absorption spectroscopy in turbid media by combined frequency-domain and steady-state methods," Appl. Opt., vol. 39, pp. 6498-507, 2000.

[6] Bevilacqua, F., You, J. S., Hayakawa, C. K. and Venugopalan, V., "Sampling tissue volumes using frequency-domain photon migration," Phys. Rev. E, vol. 69, 2004.
[7] Cerussi, A. E., et al., "Sources of absorption and scattering contrast for near-infrared optical mammography," Acad Radiol, vol. 8, pp. 211-8, 2001.
[8] Quaresima, V., Matcher, S. J. and Ferrari, M., "Identification and quantification of intrinsic optical contrast for near-infrared mammography," Photochemistry and Photobiology, vol. 67, pp. 4-14, 1998.
[9] Cerussi, A. E., et al., "Spectroscopy enhances the information content of optical mammography," J Biomed Opt, vol. 7, pp. 60-71, 2002.
[10] Pham, T. H., Coquoz, O., Fishkin, J. B., Anderson, E. and Tromberg, B. J., "Broad bandwidth frequency domain instrument for quantitative tissue optical spectroscopy," Rev. Sci. Instrum., vol. 71, pp. 2500-13, 2000.
[11] Jakubowski, D. B., et al., "Monitoring neoadjuvant chemotherapy in breast cancer using quantitative diffuse optical spectroscopy: A case study," J Biomed Opt, vol. 9, pp. 230-8, 2004
[12] Makris, A*., et al.*, "Reduction in angiogenesis after neoadjuvant chemoendocrine therapy in patients with operable breast carcinoma," *Cancer*, vol. 85, pp. 1996-2000, 1999.
[13] Brauer, M., "In vivo monitoring of apoptosis," *Prog Neuropsychopharmacol Biol Psychiatry*, vol. 27, pp. 323-31, 2003.
[14] Jagannathan, N. R., et al., "Volume localized in vivo proton mr spectroscopy of breast carcinoma: Variation of water-fat ratio in patients receiving chemotherapy," NMR Biomed, vol. 11, pp. 414-22, 1998.
[15] Merritt, S*., et al.*, "Comparison of water and lipid content measurements using diffuse optical spectroscopy and mri in emulsion phantoms," *Technol Cancer Res Treat*, vol. 2, pp. 563-9, 2003.
[16] Cerussi, A., Hsiang, D., Shah, N., Compton, M., Mehta, R., Durkin, A. F., and Tromberg, B., "Predicting response to breast cancer neoadjuvant chemotherapy using diffuse optical spectroscopy," Proceedings of the National Academy of Sciences of the United States of America, pp. accepted for publication, 2007.
[17] Choe, R., Corlu, A., Lee, K., Durduran, T., Konecky, S. D., Grosicka-Koptyra, M., Arridge, S. R., Czerniecki, B. J., Fraker, D. L., DeMichele, A., Chance, B., Rosen, M. A., and Yodh, A. G., "Diffuse optical tomography of breast cancer during neoadjuvant chemotherapy: A case study with comparison to mri," Med Phys, vol. 32, pp. 1128-39, 2005.
[18] Shah, N., Gibbs, J., Wolverton, D., Cerussi, A., Hylton, N., and Tromberg, B. J., "Combined diffuse optical spectroscopy and contrast-enhanced magnetic resonance imaging for monitoring breast cancer neoadjuvant chemotherapy: A case study," J Biomed Opt, vol. 10, pp. 51503, 2005.
[19] Zhu, Q., Kurtzma, S. H., Hegde, P., Tannenbaum, S., Kane, M., Huang, M., Chen, N. G., Jagjivan, B., and Zarfos, K., "Utilizing optical tomography with ultrasound localization to image heterogeneous hemoglobin distribution in large breast cancers," Neoplasia, vol. 7, pp. 263-70, 2005.